Geophysical Journal International

Geophys. J. Int. (2015) **203,** 856–868
GJI Seismology

doi: 10.1093/gji/ggv339

Identification of surface wave higher modes using a methodology based on seismic noise and coda waves

Diane Rivet,[1] Michel Campillo,[2] Francisco Sanchez-Sesma,[3] Nikolaï M. Shapiro[4] and Shri Krishna Singh[5]

[1]*Geoazur, University of Nice Sophia-Antipolis, CNRS, Côté d'Azur Observatory,* 250 *rue Albert Einstein, F-*06560 *Sophia-Antipolis, France. E-mail: diane.rivet@geoazur.unice.fr*
[2]*Institut des Sciences de la Terre, Université Joseph Fourier, Maison des Géosciences, BP* 53, *F-*38041 *Grenoble, France*
[3]*Instituto de Ingenieria, Universidad Nacional Autónoma de México, CU, Coyoacan,* 04510 *México, D.F., México*
[4]*Institut de Physique du Globe de Paris, Sorbonne Paris Cité, CNRS (UMR*7154*),* 1 *rue Jussieu, F-*75238 *Paris, cedex* 5, *France*
[5]*Instituto de Geofísica, Universidad Nacional Autónoma de México, CU, Coyoacan,* 04510 *México, D.F., México*

Accepted 2015 August 11. Received 2015 August 11; in original form 2015 January 8

SUMMARY

Dispersion analysis of Rayleigh waves is performed to assess the velocity of complex structures such as sedimentary basins. At short periods several modes of the Rayleigh waves are often exited. To perform a reliable inversion of the velocity structure an identification of these modes is thus required. We propose a novel method to identify the modes of surface waves. We use the spectral ratio of the ground velocity for the horizontal components over the vertical component (H/V) measured on seismic coda. We then compare the observed values with the theoretical H/V ratio for velocity models deduced from surface wave dispersion when assuming a particular mode. We first invert the Rayleigh wave measurements retrieved from ambient noise cross-correlation with the assumptions that (1) the fundamental mode and (2) the first overtone are excited. Then we use these different velocity models to predict theoretical spectral ratios of the ground velocity for the horizontal components over the vertical component (H/V). These H/V ratios are computed under the hypothesis of equipartition of a diffuse field in a layered medium. Finally we discriminate between fundamental and higher modes by comparing the theoretical H/V ratio with the H/V ratio measured on seismic coda. In an application, we reconstruct Rayleigh waves from cross-correlations of ambient seismic noise recorded at seven broad-band stations in the Valley of Mexico. For paths within the soft quaternary sediments basin, the maximum energy is observed at velocities higher than expected for the fundamental mode. We identify that the dominant mode is the first higher mode, which suggests the importance of higher modes as the main vectors of energy in such complex structures.

Key words: Surface waves and free oscillations; Site effects; Wave propagation.

INTRODUCTION

Surface wave tomography is widely used to image the structure of the Earth's superficial layers. Dispersion analysis of the surface waves provides information of the shear waves velocity in the uppermost layers. This method takes advantage of the frequency-dependent characteristic of the surface wave excitation at depth. Over the past few years ambient noise cross-correlations has been used to reconstruct Green's functions between pairs of stations and to image structures from regional to continental scales using noise in the microseismic band (Shapiro & Campillo 2004; Shapiro *et al.* 2005; Bakulin & Calvert 2006; Yang *et al.* 2007; Lin *et al.* 2008; Stehly *et al.* 2009; Yao *et al.* 2011). Surface waves are easily retrieved by ambient noise cross-correlations for two reasons, first the Green's function between two stations at the Earth's surface is dominated by surface waves, and second, ambient noise sources are generated mainly by oceanic and atmospheric interactions with the Earth's surface (Stehly *et al.* 2006; Tanimoto *et al.* 2006; Koper *et al.* 2009; Stutzmann *et al.* 2009; Landès *et al.* 2010; Hillers *et al.* 2012). Noise in the microseismic band, generated at the seafloor, mainly consists of fundamental mode surface wave energy (Bonnefoy-Claudet *et al.* 2006). Therefore, the fundamental mode is most easily recovered in noise cross-correlations between two stations.

However, recently several studies reveal the presence of higher mode surface waves in the cross-correlation (Harmon *et al.* 2007;

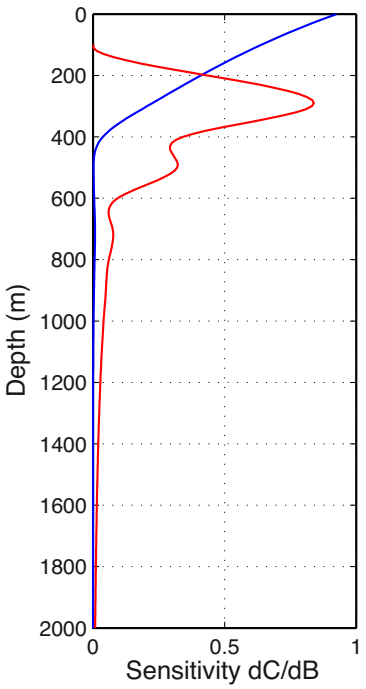

Figure 1. Depth sensitivity kernel of Rayleigh wave phase velocity of the fundamental (blue) and first overtone (red) in the velocity model below the Valley of Mexico (Table 1) and computed at 1 s periods.

Nishida *et al.* 2008; Brooks *et al.* 2009; Yao *et al.* 2011). Large velocity contrasts in the structure may induce that, one or several higher modes propagate, with more energy than the fundamental mode (e.g. Tokimatsu *et al.* 1992; Foti 2000; Zhang & Chan 2003; Liu & Fan 2012). Sedimentary basins like the Valley of Mexico (Shapiro *et al.* 2001) or in the Canterbury Basin (Savage *et al.* 2013), are sites where this phenomenon can be observed. In surface waves imaging, the Rayleigh wave dispersion curve is identified and then inverted to a 1-D velocity profile assuming laterally homogeneous medium. When dealing with ambient noise cross-correlations, it is common that the inversion of the dispersion properties is carried out assuming the dispersion curve corresponds to the fundamental mode. If this assumption of the mode is false, an erroneous identification of modes can produce serious errors in the inversion results as demonstrated by Zhang & Chan (2003), O'Neill & Matsuoka (2005). In fact, the sensitivity at depth of surface waves depends on the mode. Fig. 1 gives an example of depth sensitivity of Rayleigh waves to shear wave velocity in a velocity model below the valley of Mexico basin (Table 1), and we can see that the fundamental mode has a different sensitivity that the first overtone. Therefore, to perform reliable inversion of the velocity structure, we need to identify the dominant mode of propagation. In active experiments, dense seismic arrays are available to measure the velocity of shallow surface and with *f–k* analysis it is possible to separate modes (e.g. Nolet & Panza 1976; Horike 1985; Gabriels *et al.* 1987 and Socco & Strobbia 2004). However, the identification of the modes and the final model should be tested in a multimodal full-wavefield forward modelling (Xia *et al.* 2003; Socco & Strobbia 2004; O'Neill & Matsuoka 2005). Duputel *et al.* (2010) suggested using group-delay time information to improve higher mode detection on arrays of high-frequency sensors. More recently Poggi & Fäh (2010) and later Boaga *et al.* (2013) stressed the importance of measuring radial component in linear seismic array to distinguish first-order and higher modes in the *f–k* analysis. In addition, the authors addressed in particular the issue of misidentification due to the osculation phenomenon (Zhang & Chan 2003; Malischewsky *et al.* 2008; Tuan *et al.* 2011) and used ellipticity analysis to detect the shift of energy between fundamental and first higher mode. At lower frequency, when using seismological network, we rarely benefit from dense spatial sampling of the wavefield to consider the *f–k* approach. Wathelet (2005) proposed to test different modes of Rayleigh waves in the inversion procedure of a single dispersion curve. For a robust identification of the modes these strategies require intensive computing and a precise prior knowledge of the velocity model. The method we propose identifies the modes based on an independent seismic observation: the spectral ratio of the horizontal components over the vertical component (H/V) of the ground motion measured on seismic coda. Although microtremors (ambient noise) records are generally used to measure H/V, in this exercise we prefer to use seismic coda because the equipartition is reached while for microtremors in many instances, the apparent lack of isotropy has raised as a proof of its non-diffusive character (Mulargia 2012). The method presented in details in this paper is summarized by the following steps: (1) measuring a dispersion curve for a given pair of stations; (2) inverting the measured dispersion curve with assuming different modes (e.g. fundamental mode, first overtone, second overtone, etc.) to obtain different families of velocity models for each hypothesis; (3) computing synthetic H/V ratios following the approach of Sánchez-Sesma *et al.* (2010) and Sánchez-Sesma *et al.* (2011b) for the different velocity models; (4) estimating the H/V on the coda of several earthquakes recorded by the seismic stations and (5) comparing the synthetic and the observed H/V for the two stations that were used in the correlation. A good match between the observed H/V and a given synthetic H/V assuming a given dominant mode indicates which mode carries the energy and consequently which velocity model is correct.

Table 1. Initial velocity model bellow the Valley of Mexico.

Thickness (km)	V_P (km s^{-1})	V_S (km s^{-1})	Density (g cm^{-3})
0.35	1.5	1.20	2.05
0.20	2.5	1.80	2.05
2.00	4.0	2.70	2.20
5.00	5.3	3.05	2.40
12.00	5.7	3.30	2.40

We applied this method to identify the Rayleigh wave modes in the sedimentary basin of the Valley of Mexico. The Valley of Mexico was formed in an extensive deformation of the trans-Mexican volcanic belt since late Miocene. A recent soft lake sediments deposit recovers the basin with a thin clay layer and plays a role in the amplification of the seismic signals (see Singh *et al.* 1995 for a review). The iso-contours of the depth of the lakebed (Avilés & Pérez-Rocha 2010) are indicated in Fig. 2.

Despite the development of numerical modelling (Singh *et al.* 1995; Shapiro *et al.* 2002), the duration and characteristics of the observed ground motions in the Valley of Mexico are difficult to model reliably because the deep structure of the basin (up to several kilometres) is poorly constrained, in particular the shear wave velocity. Crustal models obtained by inversion of the dispersion curves of surface waves in central Mexico (Gomberg & Masters 1988; Campillo *et al.* 1996; Shapiro *et al.* 1997; Iglesias *et al.* 2010) or by tracing rays (Valdes-Gonzalez & Meyer 1996) do not resolve well the superficial and the deep structure of the valley. Receiver functions helped unifying the Mexican Volcanic Belt low velocity structure with the deeper structures such as the Moho discontinuity (Cruz-Atienza 2000; Pérez-Campos *et al.* 2008; Cruz-Atienza

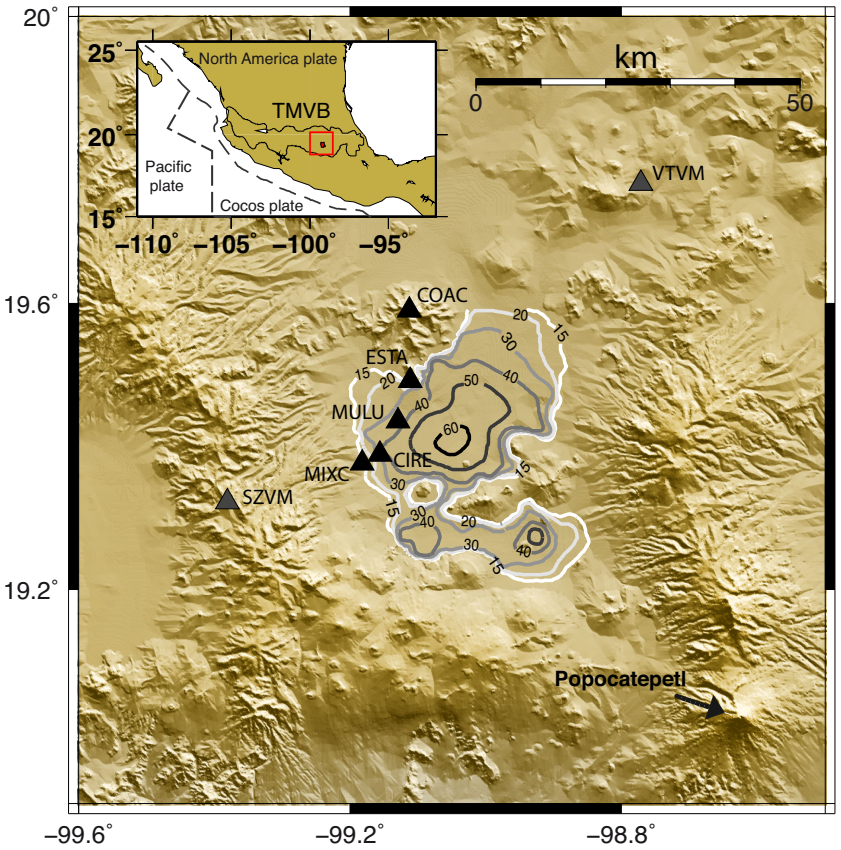

Figure 2. Inset: square is the study region in the trans-Mexican volcanic belt, Mexico. Topography of central Mexico with the Valley of Mexico indicated by the isodepths (in m) of the low-velocity deposit in the basin (the lake bed). The MASE and VMEX seismic stations used in this study are indicated by the black and grey triangles, respectively. Labels indicate the name of the seismic stations.

et al. 2010). However, these models correspond essentially to the one-dimensional character of the structure. The organization of the superficial structures is therefore poorly understood. In this context, we seek to better characterize the surface waves propagation within the Valley of Mexico.

We compute ambient seismic noise cross-correlations between seven broad-band stations. We then measure the group velocities of the reconstructed Rayleigh waves and invert them for the velocity models. Then, we use the method briefly described above to identify the dominant mode of propagation and perform reliable inversion of the velocity structure.

Data processing and noise cross-correlations

We reconstruct Rayleigh waves from cross-correlations of ambient seismic noise recorded at seven broad-band stations of the MesoAmerica Seismic Experiment (MASE) and Valley of Mexico Experiment (VMEX). The seismic sensors are of two types: Guralp CMG40 and CMG-6TD, both have a flat spectral response up to 30 s period. Daily cross-correlations are computed in the frequency domain and then stacked over 2 yr for the MASE stations and over 1 yr for the VMEX stations. Before being correlated, the recorded seismic noise is first whitened in the frequency domain, and we then apply a 1-bit normalization in the time domain, which is to keep only the sign of the signal. For each pair of stations, because of the lower quality of the transverse components, only ZZ cross-correlations from vertical components were calculated resulting in the recovery of the Rayleigh waves.

For the SZVM and VTVM inter-stations path of ∼80 km and for the MIXC-ESTA path of ∼7 km (Fig. 2), the cross-correlation functions were filtered in different period bands: 2–5, 5–10 and 10–20 s for SZVM-VTVM and 0.5–1, 1–2, 2–3 and 3–5 s for MIXC-ESTA (Fig. 3). We observe the dispersive character of the reconstructed Rayleigh waves, with the longer period waves preceding the short period waves, for both long and short interstation distances. The Rayleigh wave dispersion presented in Fig. 3 suggests that we can use the cross-correlation functions to image the velocity structure of the valley of Mexico based on the analysis of the dispersion characteristics.

In the following, we consider Rayleigh waves computed between two stations with sufficient signal-to-noise ratio (SNR > 8) to measure group velocity dispersion curves. The amplitude of the signal is measured at the time of the maximum of the envelope signal of the correlation, which gives us a good approximation of the arrival time of the Rayleigh wave, while the amplitude of the noise is measured on a window of 40 s long, between 80 and 120 s of the correlation signal.

Dispersion of Rayleigh waves from noise cross-correlations

We use the frequency–time analysis (Levshin *et al.* 1989) to measure group velocities of surface waves on noise cross-correlations. First to extract group velocity measurements, we narrow band-pass filter the cross-correlation and then calculate the envelope of the signals and measure the time at its peak amplitude. In a time-frequency

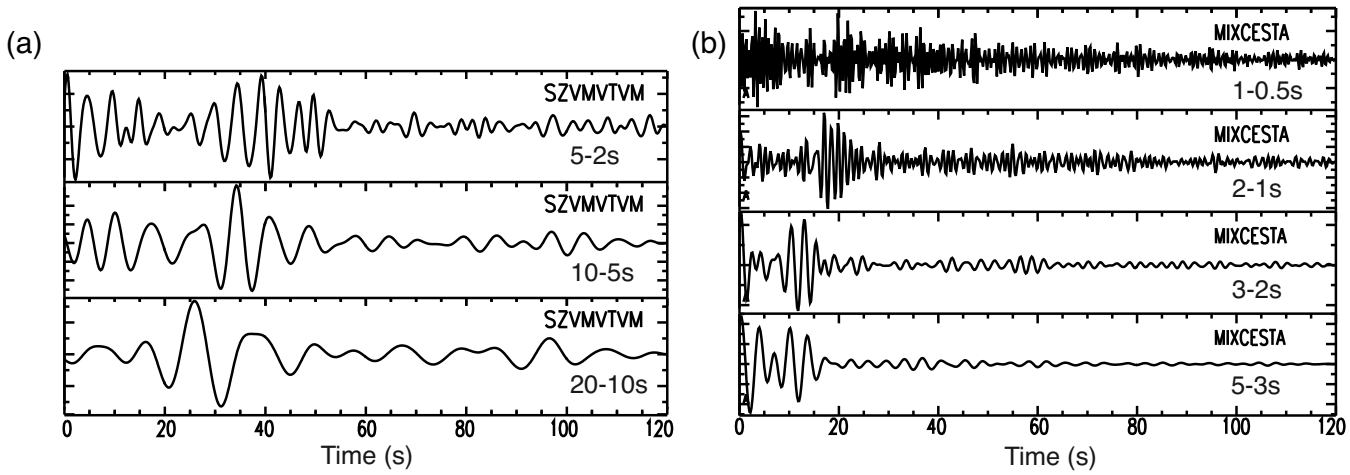

Figure 3. Cross-correlations between (a) SZVM and VTVM stations from five months of noise, and between (b) ESTA and MIXC stations from 12 months of noise, filtered for different period band and computed for the vertical components of noise records.

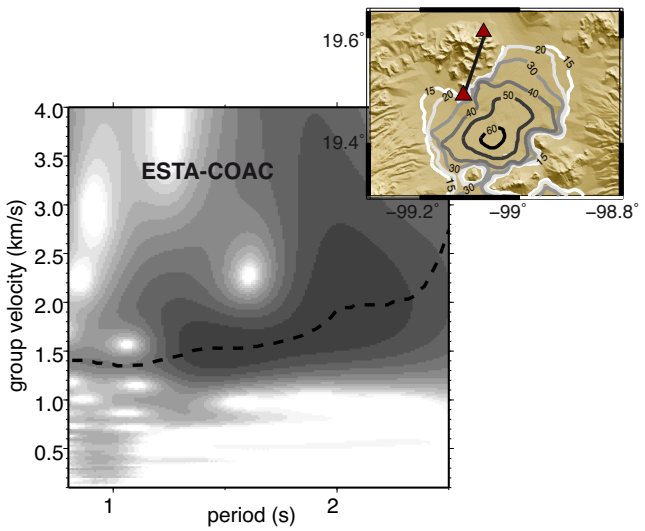

Figure 4. Period-velocity diagrams used to identify the Rayleigh waves and their group velocity dispersion, computed between stations ESTA and COAC located outside the sedimentary basin (triangles on the map). The dashed line represents the dispersion curve of the dominant energy level.

representation, the position of the maximum amplitude of the envelope of the Rayleigh wave at each frequency defines the dispersion curve of the group velocity.

First, we are interested in identifying the differences between surface wave propagation outside and inside the quaternary sedimentary basin. We will focus specifically on the 0.5–3 s period band for which the surface waves are sensitive to the structure of the sedimentary basin. We compute cross-correlations between four MASE broad-band sensors. Among them COAC station is located outside of the sedimentary basin (∼15 km north of the basin), ESTA station is located at the northern border of the basin and MULU, CIRE and MIXC stations are located inside the basin.

For paths outside the Valley of Mexico, like the ESTA-COAC stations path (Fig. 4), the dominant mode of Rayleigh waves travels at 1.5 km s^{-1} at period $T = 1$ s, and at 2 km s^{-1} at period $T = 2$ s. This mode corresponds to the velocity expected for the fundamental mode of Rayleigh waves outside the sedimentary basin. For paths within the soft quaternary basin, the group velocity analysis shows different features. The dispersion of the group velocity of the cross-correlation functions was measured for four stations paths MIXC-ESTA, MIXC-MULU, CIRE-MULU and CIRE-ESTA, all located within the lake-bed zone (Fig. 5). From the period-group velocity diagrams, we observe that the dominant energy for $T > 2$ s travels at about 0.9 km s^{-1} in the basin, against 2 km s^{-1} outside the basin. Moreover, for all four paths, we observe another maximum with velocities about 0.3 km s^{-1} at periods between 1.5 and 3 s. Finally, for the MIXC-MULU and CIRE-ESTA paths only the faster maximum can be identified with a group velocity of the order of 1.8 km s^{-1} for periods between 1.5 and 2 s. Paths between stations considered here cross different parts of the sedimentary basin, which explains the observed variability of the energy levels. By comparing Figs 4 and 5, we note that, as expected, all the dominant dispersion curves within the basin are much slower than the one observed outside the basin. The sedimentary basin plays a decisive role in the propagation of Rayleigh waves in the period band considered in this study. Besides, for all inter-stations paths, the maximum energy is observed at velocities (0.9 km s^{-1} for $T = 2$ s) higher than expected for the fundamental mode from *in situ* measurements (e.g. Chávez-García & Bard 1994). This observation suggests the importance of higher modes as the main vectors of energy in the basin of the Valley of Mexico. At period considered here, the sensitivity of the fundamental mode to the *S*-wave velocity is maximal at the free surface, where the speed is the slowest (0.2 km s^{-1}) and the attenuation the highest. For the fundamental mode the displacement at depth decreases more rapidly for than for the higher modes. In these conditions, it seems that the energy transport through the Rayleigh wave fundamental mode is ineffective.

These results are consistent with previous studies (e.g. Shapiro *et al.* 2001) and highlight the importance of the deep structure of the basin that controls the dispersion of the higher modes surface waves. The use of ambient seismic noise to recover shallow crustal structures in the Valley of Mexico seems feasible. However, before we can determine the velocity structure beneath the basin, it is necessary to identify the dominant modes of propagation of surface waves.

Inversions of the dispersion curves assuming a given mode

Velocity models were estimated using a neighbourhood algorithm developed by Wathelet (2008) and implemented in the GEOPSY

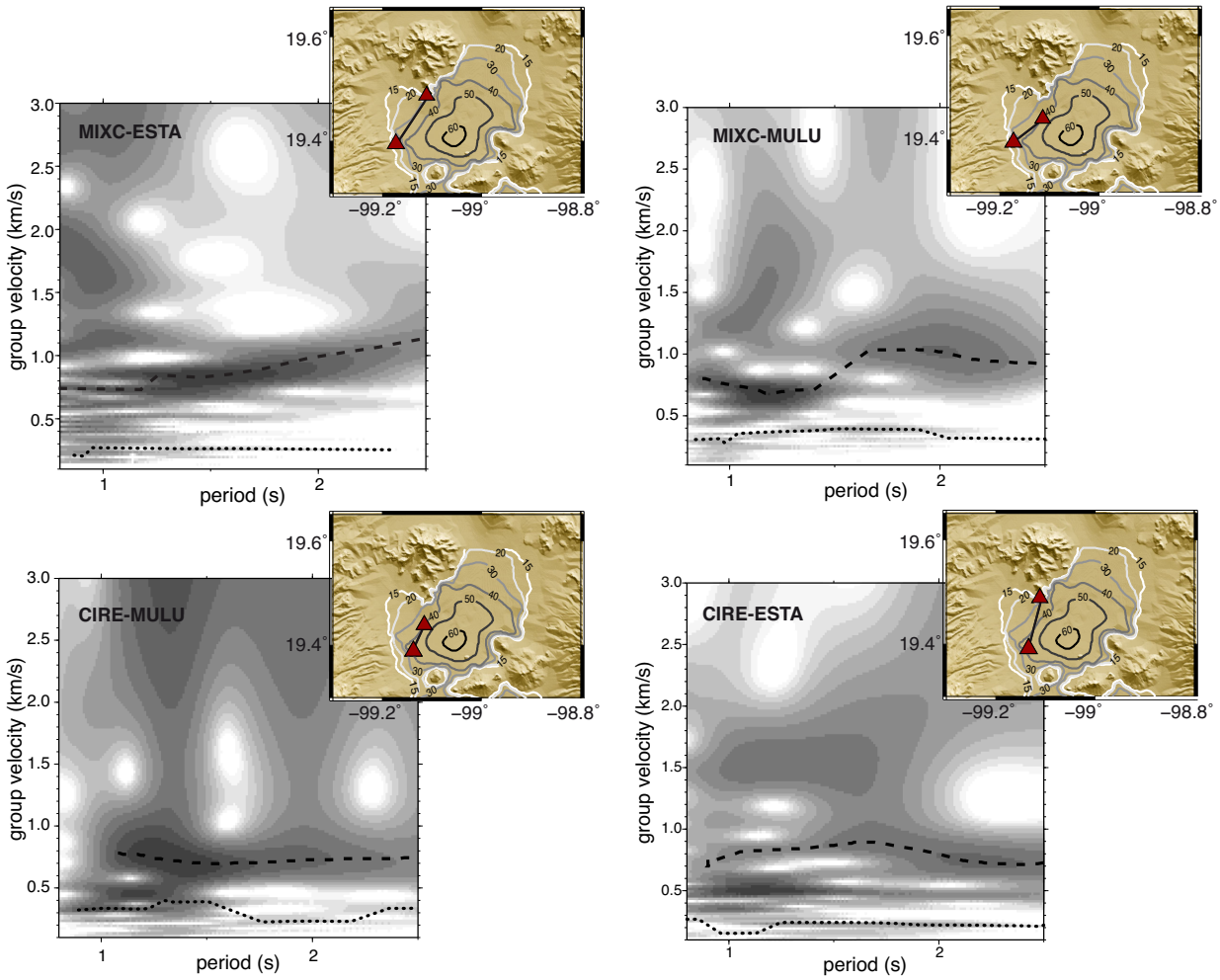

Figure 5. Period-velocity diagrams calculated for four inter-stations paths located within the sedimentary basin of the Valley of Mexico (MIXC-ESTA, CIRE-MULU, MIXC-MULU and CIRE-ESTA). Dashed and dotted curves represent the dominant energy level and a slower energy level observed for slower group velocities, respectively.

software. Because the dominant mode observed in the dispersion diagrams is not yet identified, we invert the highest energy dispersion curves measured from the cross-correlations assuming that they correspond either to the fundamental mode or to the first higher mode. For each pair of stations we will thus obtain two families of velocity models, each family corresponding to the hypothesis of the dominant mode assumed.

We use a 1-D velocity model as *a priori* information to constrain the structure below the valley (Table 1). This velocity model was modified from the model used by Shapiro *et al.* (2001) in order to better fit the dispersion curves computed for the path outside the lake-bed zone, for short period (0.5–3 s) and longer period (3–10 s) for the SZVM-VTVM dispersion curves. The model takes into account for the deeper portion, the regional structure determined by Campillo *et al.* (1996). The shallower structure is made of two layers of 2 km thickness each with lower velocity characteristic of volcanic rocks of the Miocene (Havskov & Singh 1977). Above, the quaternary sedimentary basin has a thickness of 500 m (Suarez *et al.* 1987) and on top of it is the lake sediments with a maximum thickness of ∼60 m.

We invert the dispersion curve of the reconstructed Rayleigh wave for the MIXC-ESTA and CIRE-MULU stations paths. For these paths we can clearly identify the dispersion of the dominant mode. MIXC, CIRE and ESTA stations are located close to the edge of the basin while MULU is located on the deeper part of the basin. Because the sensitivity of Rayleigh waves at period considered in this study is limited to the top 2 or 3 km of the crust, for depth greater than 3 km below we fix the velocity at 2.8 km s^{-1} in a half-space. Furthermore, we invert only for the *S*-wave velocity, the *P*-wave velocity and the density are kept constant. Assuming that *P*-wave velocity and density are constant can be considered as a first order approximation. Lontsi *et al.* (2015) have found some sensitivity of H/V to *P*-wave velocity but to a lesser extent than for *S* wave.

For a given station pair, we first invert the selected dispersion curve assuming that it corresponds to the fundamental mode and we then repeat the inversion, assuming that the dominant mode observed in dispersion curve is the first overtone. Fig. 6 shows the eigenfunctions calculated for the fundamental and the first higher modes of Rayleigh waves at 2 s period. These eigenfunctions give theoretical distributions of displacement with depth for each mode. It can be seen that the displacement decreases more rapidly for the fundamental modes than for the first higher mode. Therefore inverting either for the fundamental mode or for a higher mode changes the sensitivity at depth and where the *S*-velocity will be best constrained.

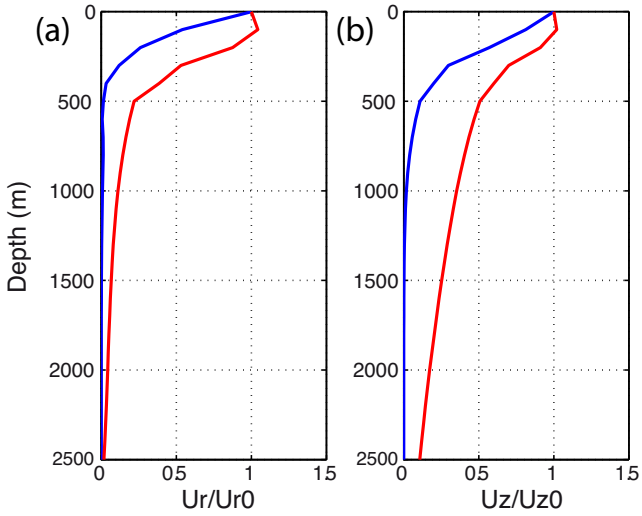

Figure 6. Eigenfunctions of the fundamental (blue) and the first higher modes (red) of Rayleigh waves. (a) Normalized radial-component and (b) vertical-component estimated at 2 s for the initial velocity model given in Table 1.

Fig. 7 presents the observed and modelled MIXC-ESTA dispersion curves (Fig. 7a) and the generated *S*-wave velocity profiles (Fig. 7b). We then repeat the inversion, assuming that the dominant mode observed in the MIXC-ESTA dispersion curve is the first overtone. Figs 8(a) and (b) show the modelled dispersion curves for the fundamental mode and the first higher mode, respectively. Fig. 8(c) presents the generated velocity models from which the synthetic dispersion curves were computed. We repeat the same steps for CIRE-MULU dispersion curve. Fig. 9 presents the observed and modelled CIRE-MULU dispersion curves and the generated *S*-wave velocity profiles assuming the dispersion curves is the fundamental mode, while Fig. 10 shows modelled and observed dispersion curves and velocity models assuming the dispersion curves is the first higher mode.

We observed that both inversions succeed in fitting the observed dispersion curves equally well. The two best velocity models assuming different modes for the MIXC-ESTA and CIRE-MULU cross-correlations, are however quite different: for MIXC-ESTA the *S*-velocity profile, under the first mode assumption, is slower on average than the one obtained under the fundamental mode assumption, for CIRE-MULU, under the first mode assumption, the shallowest layer between 0 and 300 m is slower while at depth the velocity is larger than the velocity profile obtained under the fundamental mode assumption. Those non-negligible differences in the velocity profiles depending on which modes we consider, highlight that it is crucial to identify correctly the dominant mode to resolve properly the crustal structure.

Identifying the dominant mode of surface waves using H/V spectral ratios

To identify the modes of the surface waves and to test the validity of the velocity models, we use H/V spectral ratios. The H/V measurements are generally obtained by the ratio of the Fourier amplitude spectra of the horizontal component (H) and the vertical

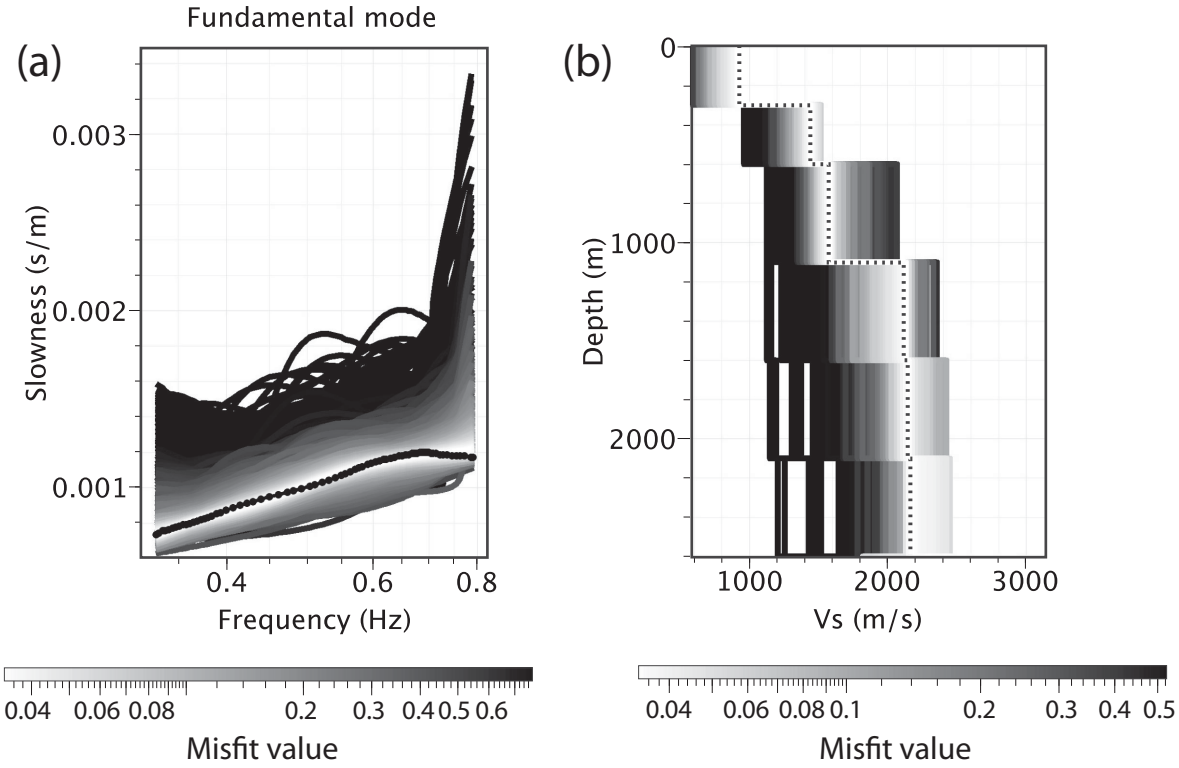

Figure 7. Velocity models inverted from the dispersion curve of the dominant mode of the Rayleigh wave for MIXC-ESTA path, assuming that this mode is the fundamental mode. (a) Grey lines are the computed fundamental mode dispersion curves for models selected during inversion; the dotted black line shows the observed dispersion curve. (b) Generated velocity profiles from which the synthetic curves were computed. The velocity profiles in white, with smaller misfit value, better explain the observed dispersion curves; the dotted black line indicates the best velocity model.

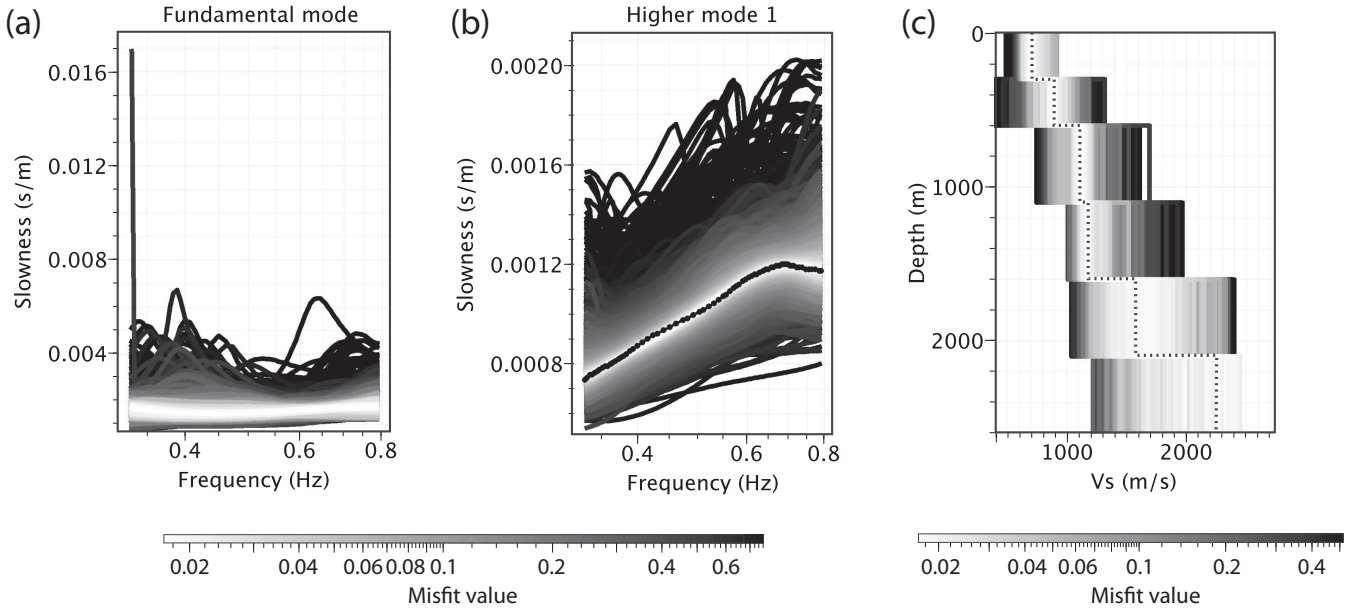

Figure 8. Velocity models inverted from the dispersion curve of the dominant mode of the Rayleigh wave for MIXC-ESTA path, assuming that this mode is the first higher mode. (a) Grey lines are the fundamental mode dispersion curves for models selected during inversion. (b) Grey lines are the first higher mode dispersion curves for models selected during inversion; the dotted black line shows the observed dominant dispersion curve. (c) Generated velocity profiles; the dotted line indicates the best velocity model.

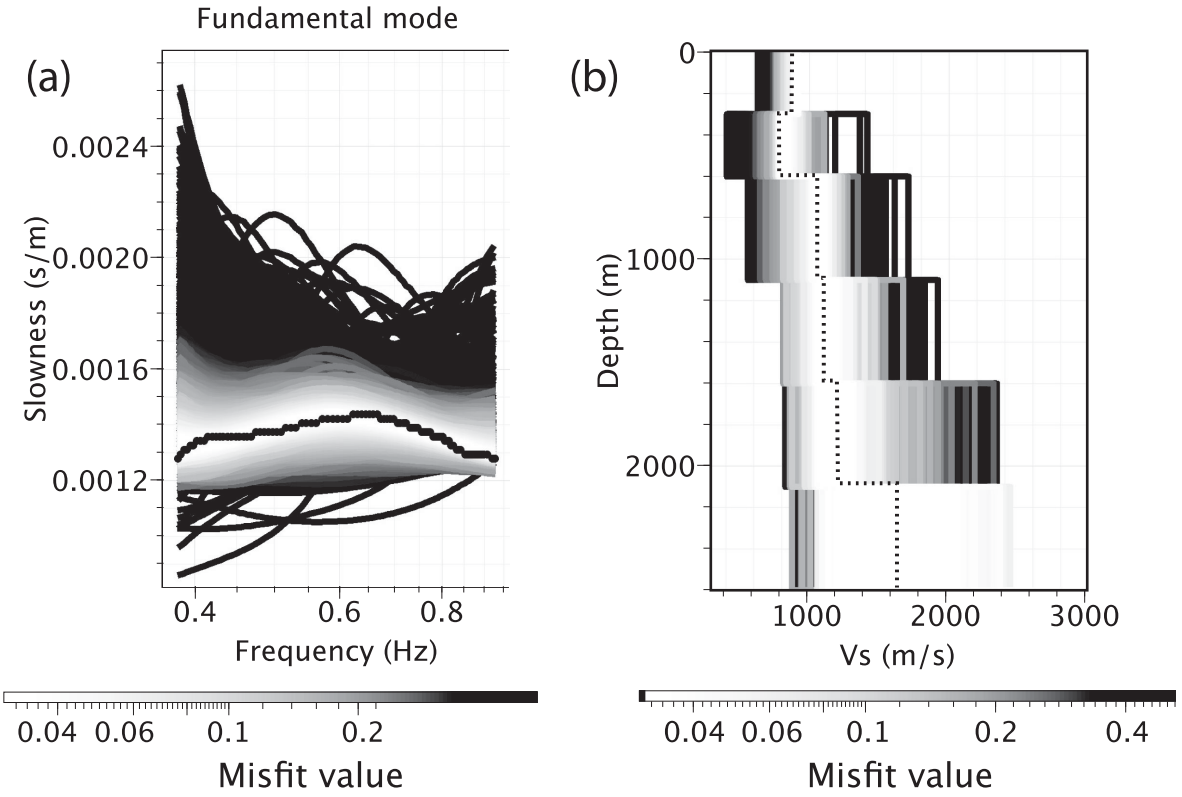

Figure 9. Same as Fig. 7 but for CIRE-MULU path.

component (V) (eq. 1) of the ambient noise recorded at a single station Nakamura (1989).

$$H/V = \frac{\sqrt{|N|^2 + |E|^2}}{|V|}, \tag{1}$$

with N the north–south, E the east–west and V the vertical components of the ground motion. This ratio depends on the resonance frequency of the medium (Fäh *et al.* 2001; Malischewsky & Scherbaum 2004), but is sometimes interpreted as related to the ellipticity of surface waves (Fäh *et al.* 2003). It is frequent to compute H/V as the average of ratios of spectral amplitude for a set

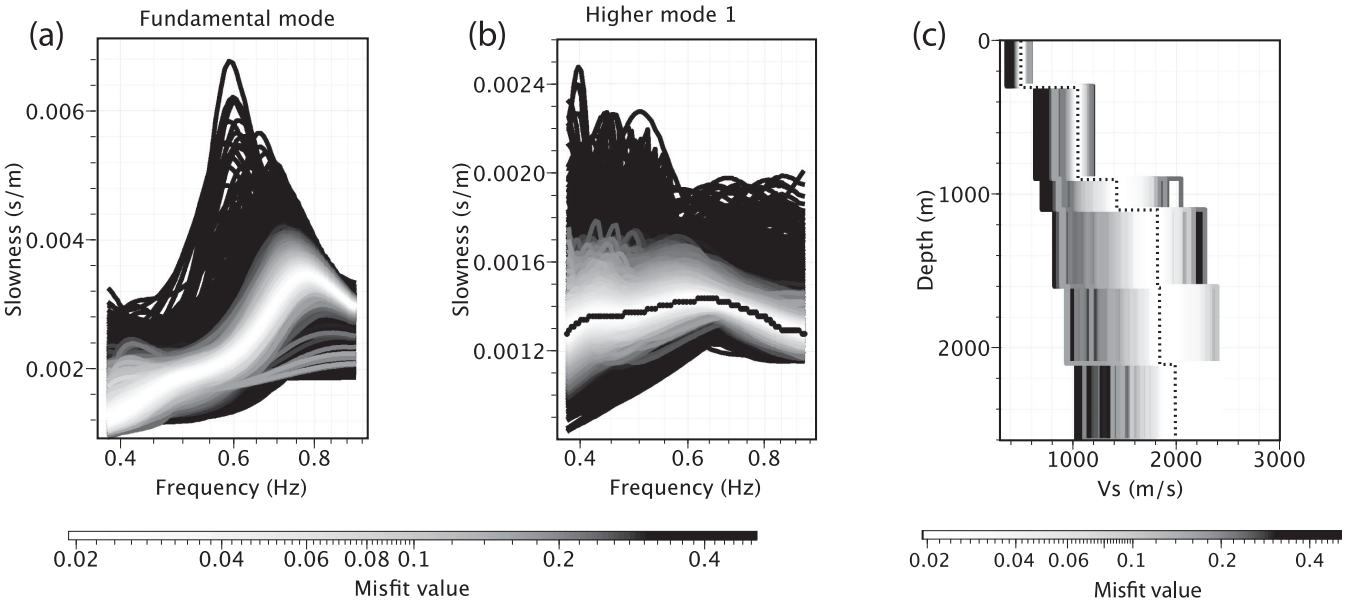

Figure 10. Same as Fig. 8 but for CIRE-MULU path.

of selected windows. However, for theoretical reasons we favour to compute H/V as the ratio of spectral amplitude averages as proposed by Arai & Tokimatsu (2004) averages of ratio of spectral amplitude In this study, the spectral ratio H/V is calculated from the coda waves of earthquakes. In the theory developed by Margerin *et al.* (2001, 2009) and Sánchez-Sesma *et al.* (2011b), it is possible to identify the H/V spectral ratio from a diffuse and equipartitioned wave field such as the coda of earthquakes produced by the multiple scattering of seismic waves. In this case H/V is a characteristic of the elastic properties of the medium. Apart from early arrivals, the energy decay of the coda can be approximated by a diffusive equation and is characterized by the stabilization of the shear (W^s) to compressional (W^P) energy ratio (W^s/W^P) resulting from equipartition of the phase space (Weaver 1982; Weaver 1990; Ryzhik *et al.* 1996; Hennino *et al.* 2001). This equipartition implies that in a diffusive regime while the energies of the shear and compressional waves decrease with time, their ratio (W^s/W^P) tends to stabilize to a constant. Equipartition has been observed numerically by Margerin *et al.* (2000) and latter in seismic data by Shapiro *et al.* (2000). In Mexico, the stabilized energy ratio (W^s/W^P) happened to be in very good agreement with the theoretical estimations for surface and body waves (Hennino *et al.* 2001). Furthermore, the equipartition of the coda above 1 Hz is reached very quickly which indicates the dominance of the multiple scattering regime in the crust (Hennino *et al.* 2001).

The condition of equipartition allows for two uses of diffuse fields. First, in the case of a diffuse field such as the seismic coda, it is possible to retrieve the imaginary part of the Green's function from the cross-correlation of the coda recorded at two stations (Campillo & Paul 2003; Sánchez-Sesma *et al.* 2008). The general expression of the average cross-correlations of motions at point X_A and X_B for a 3-D diffuse, equipartitioned, harmonic displacement vector field $u_i(x,\omega)$, within an elastic medium can be written as (e.g. Sánchez-Sesma & Campillo 2006):

$$u_i(X_A,\omega)\,u_j^*(X_B,\omega) = -2\pi E_s k^{-3}\mathrm{Im}\left[G_{ij}(X_A,X_B,\omega)\right], \qquad (2)$$

with $G_{ij}(X_A,X_B,\omega)$ = Green's function = displacement at X_A in the direction i produced by an unit harmonic load at X_B in the direction $j = \delta_{ij}\delta(X,X_B)\,e^{-i\omega t}$, i = imaginary unit, ω = circular frequency, $k = \omega/\beta$ = wave number, with β = shear wave velocity, $E_s = \rho\omega^2 S^2$ = average energy density of shear waves with ρ = mass density and S^2 = average spectral density of shear waves. The asterisk $*$ indicates the complex conjugate and the bracket the azimuthal average.

Second, the average autocorrelation of motion for a given direction m at a given point is proportional to the directional energy density (DED; Sánchez-Sesma *et al.* 2008; Perton *et al.* 2009). If we assume $X_B = X_A$ in eq. (2), we have the energy density at point X_A:

$$\begin{aligned} E_m(X_A) &= \rho\omega^2 u_m(X_A)\,u_m^*(X_A) \\ &= -2\pi\mu E_S k^{-1} \times \mathrm{Im}\left[G_{mm}(X_A,X_A)\right]. \end{aligned} \qquad (3)$$

We thus retrieve from the directional energy density at a given direction m, the imaginary part of the Green's function at the position X_A (Margerin 2008; Perton *et al.* 2009; Sánchez-Sesma *et al.* 2011a), linking the averaged energy spectral ratio of a diffuse wave field to the intrinsic property of the medium expressed through the Green's function. Assuming a diffuse field, we can write the stabilized spectral densities as a function of the directional energy densities. The H/V ratio results:

$$[H/V](\omega) = \sqrt{\frac{E_1(x,\omega)+E_2(x,\omega)}{E_3(x,\omega)}}, \qquad (4)$$

where E_1, E_2 and E_3 are the DEDs and the subscripts 1 and 2 refer to horizontal and 3 to vertical components. The H/V spectral ratio eq. (4), using eq. (3), is written by means of:

$$[H/V](\omega) = \sqrt{\frac{\mathrm{Im}\left[G_{11}\right](x,x;\omega)+\mathrm{Im}\left[G_{22}\right](x,x;\omega)}{\mathrm{Im}\left[G_{33}\right](x,x;\omega)}}. \qquad (5)$$

The H/V spectral ratio thus depends on the contribution of all waves existing in the Green's function: Rayleigh, Love and body waves. By estimating the H/V ratio on the coda of earthquakes, we thus expect to retrieve information about the structure beneath the station.

We compute the H/V spectral ratios from the coda of several earthquakes with sufficient signal to noise ratio and which

Table 2. Earthquakes used for the estimation of the H/V spectral ratio on coda.

Place	Date	Time	Lat (°)	Long (°)	Depth (km)	M_w
Kuril Islands	2006/11/15	11:14:13	46.59	153.27	10	8.3
Kuril Islands	2007/01/13	04:23:21	46.23	154.55	10	8.1
Tonga	2006/05/03	15:26:40	−20.19	−174.12	55	8.0
Pakistan	2005/10/08	03:50:39	34.46	73.58	19	7.6
Baja California	2006/01/04	02:32:31	28.1	−112	10	6.7
Offshore Guatemala	2007/06/13	19:29:40	13.56	−90.66	23	6.7
Michoacán, Mexico	2006/08/11	14:30:50	18.54	−101	56	6.1
Guatemala	2006/12/03	20:52:15	13.97	−91.22	61	6
Off the coast of Jalisco, Mexico	2006/04/04	02:30:28	18.76	−106.99	33	6.0
Gulf of Mexico	2006/09/10	14:56:07	26.25	−86.63	14	5.9
Gulf of California	2007/02/25	15:00:41	26.18	−110.42	10	5.9
Gulf of California	2007/03/13	02:59:04	26.22	−110.6	26	5.9
Gulf of Mexico	2007/05/23	19:09:15	21.892	−96.359	10	5.6

characteristics are listed Table 2. We processed several recordings of events including large and distant earthquakes as well as regional events to ensure that the observed H/V is stable. The frequency content of codas for teleseimic and regional events are different, however at a given frequency the H/V ratio is similar for both type of events. Because the duration of the coda varies as a function of the period, that is coda at long period lasts longer than the coda at short period, we measured the spectral amplitude on time windows whose duration was defined for each period band. At a given period band the coda time window initiates for an amplitude of coda lower than eight times the maximum amplitude of the earthquake signals and ends when the coda amplitude reaches two times the average noise level measured on 4 hr window preceding the earthquake. This insures that the spectral amplitude at a given period is estimated on the coda and not on the noise. Fig. 11 shows an example of a coda time window selection depending on the period band. In the

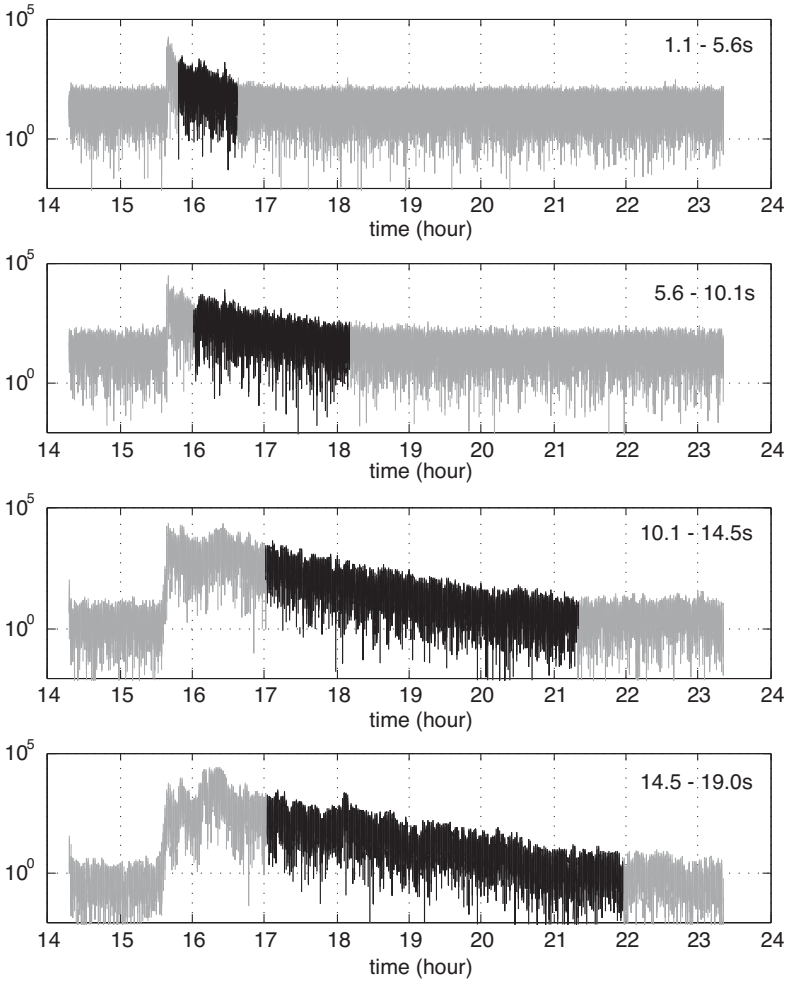

Figure 11. Amplitude of the coda of the 2006-05-03 $M_w = 8.0$ Tonga earthquake recorded at ESTA station, filtered in different period bands labelled in the top-right hand corner of each plot. Black signal shows the portion of the signal we select to compute the H/V spectral ratio.

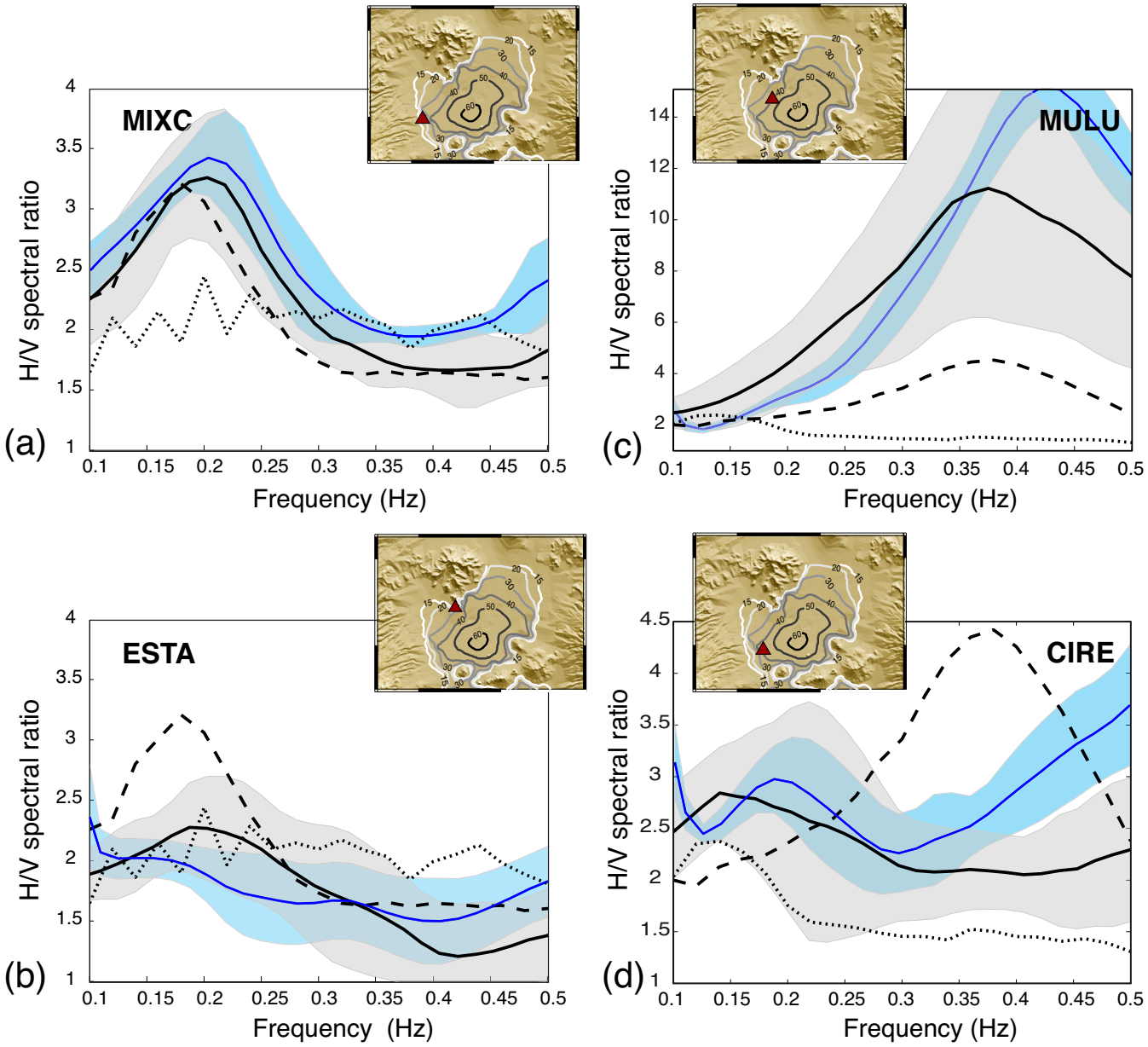

Figure 12. Comparison between the observed and estimated H/V spectral ratios measured at (a) MIXC (b), ESTA, (c) MULU and (d) CIRE stations. Observed H/V ratios averaged for all earthquakes listed Table 2 are indicated by the black solid lines, and the respective standard deviation is shown by the grey shaded area. The blue curves and shaded areas indicate the H/V ratios measures on microtremors averaged for 8 d of seismic noise records and its standard deviation. The calculated H/V spectral ratios for the (a–b) MIXC-ESTA and (c–d) CIRE-MULU stations path, from the different velocity models assuming that the dominant mode is the fundamental mode or the first higher mode of the Rayleigh wave are shown by the dotted curve and dashed curve, respectively.

following we considered H/V ratio measured for frequency between 0.1 and 0.5 Hz. At frequency smaller than 0.1 reliable H/V ratios can hardly be measured (Strollo *et al.* 2008; García-Jerez *et al.* 2013) because different phenomena such as the ground tilting of the station due to near load effect (Wielandt & Forbriger 1999; Forbriger 2006) or atmospheric pressure variations and wind (De Angelis & Bodin 2012) dominate the measure of H/V ratio.

We also estimate H/V ratio on microtremors measured on a 1 hr moving window from midnight to 6 a.m. for 10 d, and compare with H/V ratios measured on seismic codas. Because H/V is more commonly estimated on noise than on seismic coda, we test is it would be possible to replace for the mode identification the H/V ratio measured on coda by the one measured on noise. Even if equipartition cannot be proved, recent work on the statistical properties of seismic noise shows that, under a wide variety of circumstances, the emergency of Green's function is effective after an adequate averaging process is performed (Pilz & Parolai 2014).

From eq. (5), theoretical H/V spectral ratios are computed provided a 1-D velocity model. We compare the observed values of H/V spectral ratio on both coda an microtremors with the theoretical H/V estimated from the velocity models previously deduced from the surface wave dispersion curves when assuming a particular mode. Fig. 12 presents for the MIXC-ESTA and CIRE-MULU paths (1) the theoretical H/V ratios computed for the two velocity models assuming, respectively that the dominant mode is the fundamental mode and the first higher mode of the Rayleigh wave

and (2), the averaged H/V ratios measured from the seismic codas and microtremors. For MIXC station (Fig. 12a), we observe a good match between the observed H/V ratio and the computed ratio under the first higher mode assumption. This strongly suggests that the dominant mode of the Rayleigh wave is the first higher mode. For ESTA station (Fig. 12b), the observed H/V ratio differs from the two computed ratios. However both the observed H/V ratio and the ratio obtained for the first higher mode assumption presents amplification at 0.2 Hz. For MULU station located atop the deeper part of the basin (Fig. 12c), we observe a strong amplification at 0.4 Hz for both the observed H/V ratio and the computed ratio under the first higher mode assumption although the amplitude of the synthetic H/V is not recovered. The amplitude discrepancy may be due to the top most superficial low-velocity layer that amplifies the seismic waves and that is not taken into account in our H/V modelling. This observation is in agreement with results of Shapiro *et al.* (2001) at station ROMA located 2 km west of MULU and for which they observed amplification at 0.4 Hz corresponding to the first higher mode of Rayleigh waves. Finally for CIRE station (Fig. 12d), we observe a small amplification at 0.15 Hz on H/V estimated on earthquake coda, which corresponds quite well with the amplification observed for the fundamental mode. However in this later case the H/V estimated on microtremors has different features with a small amplification as 0.2 Hz and a larger one for a frequency larger to 0.5 Hz. The differences between the observed and computed H/V we observed at ESTA and CIRE stations, arise from the fact that the observed H/V is a local measurement at each station while the computed H/V is obtained from the average velocity model between the two stations. Nonetheless the comparison between modelled and measured H/V ratios help us to identify the modes unambiguously and, consequently, to recover the velocity model of the structure. In addition we verified that H/V ratios measured on earthquakes coda and on microtremors are in good agreement. However when amplification is low, differences between equipartitioned coda and noise are visible. Besides urban area such as Mexico City with relatively low quality data with strong day–night amplitude variations, spikes, electrical glitches, the selection of the time window of microtremors is crucial to measure a reliable H/V ratio.

DISCUSSIONS AND CONCLUSIONS

Sedimentary basins control the ground motion by trapping and amplifying seismic waves. Understanding and characterizing wave propagation within sedimentary basin is fundamental to (1) imaging a detailed crustal structure and (2) for accurate strong ground motion prediction.

To characterize the velocity structure, it is crucial to identify properly surface wave mode. Surface waves, depending on their mode, will not travel the same way across the basin. In fact, the difference between fundamental and higher modes is that the energy of the fundamental mode is concentrated in the superficial layers, while the higher modes propagate deeper and are therefore less affected by the clay sediment and low Q.

Using H/V spectral ratios observed on seismic codas compared with ratios calculated from different structural models we identify the dominant mode. Application of this approach allowed us to conclude that the dominant mode of propagation of short-period Rayleigh waves within the Valley of Mexico is the first overtone, which confirms the results of Shapiro *et al.* (2001). Higher modes surface wave also dominate in Canterbury region of New Zealand (Savage *et al.* 2013). For Kanto the fundamental mode dominates (Denolle *et al.* 2014). However in this latter case, the analysis was only performed with ZZ components and that Savage *et al.* (2013) show that the first overtone could be stronger on the RR components, such that the Kanto basin may see higher mode if horizontal components are analysed. The geological conditions that make that, in one case the fundamental mode dominates and on another case the higher mode dominates, need to be determined.

Because the fundamental mode tend to be trapped in the shallower sediment layers, when the fundamental mode is dominant, a fine description of the edge geometry of the basin and thickness of the top layer of sediments are required to predict accurately the ground motion. On the other hand, when higher modes are dominant, the deeper layers need to be accurately constrained. In the latter case the role of the superficial low-velocity layer is to amplify the seismic waves at the fundamental period of the site (Shapiro *et al.* 2001).

Surface wave mode identification is also important for practical aspects for engineering purpose in designing of pipelines and tunnels (see e.g. Bodin *et al.* 1997; Singh *et al.* 1997) because the amplitude of the strain and its distribution for the higher mode differs from those of the fundamental mode.

ACKNOWLEDGEMENTS

This study was supported by the Agence National de la Recherche (France) under the contract RA0000CO69 ‘G-GAP’, by the European Research Council Advanced Grant 227507 «Whisper ». Diane Rivet held a fellowship from Region Rhône-Alpes. The work of NMS was supported by the Russian Science Foundation (grant 14-47-00002). We thank Robert Clayton and Luis Quintanar for access to seismic data.

REFERENCES

Arai, H. & Tokimatsu, K., 2004. S-wave velocity profiling by inversion of microtremor H/V spectrum, *Bull. seism. Soc. Am.,* **94,** 53–63.

Avilés, J. & Pérez-Rocha, L.E., 2010. Regional subsidence of Mexico City and its effects on seismic response, *Soil. Dyn. Earthq. Eng.,* **30,** 981–989.

Bakulin, A. & Calvert, R., 2006. The virtual source method: theory and case study, *Geophysics,* **71**(4), SI139–SI150.

Boaga, J., Cassiani, G., Strobbia, C.L. & Vignoli, G., 2013. Mode misidentification in Rayleigh waves: ellipticity as a cause and a cure, *Geophysics,* **78**(4), EN17–EN28.

Bodin, P., Gomberg, J., Singh, S.K. & Santoyo, M., 1997. Dynamic deformation of shallow sediments in the Valley of Mexico, part I: Three-dimensional strains and rotations recorded on a seismic array, *Bull. seism. Soc. Am.,* **87,** 528–539.

Bonnefoy-Claudet, S., Cotton, F. & Bard, P.-Y., 2006. The nature of noise wavefield and its applications for site effects studies: a literature review, *Earth-Sci. Rev.,* **79**(3), 205–227.

Brooks, L.A., Townend, J., Gerstoft, P., Bannister, S. & Carter, L., 2009. Fundamental and higher-mode Rayleigh wave characteristics of ambient noise in New Zealand, *Geophys. Res. Lett.,* **36,** L23303, doi:10.1029/2009GL040434.

Campillo, M. & Paul, A., 2003. Long-range correlations in the diffuse seismic coda, *Science,* **299,** 547–549.

Campillo, M., Singh, S.K., Shapiro, N.M., Pacheco, J. & Herrmann, R., 1996. Crustal structure south of the Mexican volcanic belt, based on group velocity dispersion, *Geof. Int. – Mexico,* **35,** 361–370.

Chávez-García, F. & Bard, P., 1994. Site effects in Mexico City eight years after the September 1985 Michoacan earthquakes, *Soil. Dyn. Earthq. Eng.,* **13,** 229–247.

Cruz-Atienza, V.M., 2000. Inversion global con algoritmos genèticos y cristalización simulada, aplicada a funciones de receptor: Modelos

estructurales de velocidades para la corteza en la República Mexicana, *Master's thesis,* Universidad Nacional Autonoma de Mexico, Mexico.

Cruz-Atienza, V.M., Iglesias, A., Pacheco, J., Shapiro, N.M. & Singh, S.K., 2010. Crustal structure below the Valley of Mexico estimated from receiver functions, *Bull. seism. Soc. Am.,* **100,** 3304–3311.

De Angelis, S. & Bodin, P., 2012. Watching the wind: seismic data contamination at long periods due to atmospheric pressure-field-induced tilting, *Bull. seism. Soc. Am.,* **102,** 1255–1265.

Denolle, M.M., Miyake, H., Nakagawa, S., Hirata, N. & Beroza, G.C., 2014. Long-period seismic amplification in the Kanto Basin from the ambient seismic field, *Geophys. Res. Lett.,* **41**(7), 2319–2325.

Duputel, Z., Cara, M., Rivera, L. & Herquel, G., 2010. Improving the analysis and inversion of multimode Rayleigh-wave dispersion by using group-delay time information observed on arrays of high-frequency sensors, *Geophysics,* **75**(2), R13–R20.

Fäh, D., Kind, F. & Giardini, D., 2001. A theoretical investigation of average H/V ratios, *Geophys. J. Int.,* **145,** 535–549.

Fäh, D., Kind, F. & Giardini, D., 2003. Inversion of local *S*-wave velocity structures from average H/V ratios, and their use for the estimation of site-effects, *J. Seismol.,* **7,** 449–467.

Forbriger, T., 2006. Low-frequency limit for H/V studies due to tilt – tilt induced acceleration versus inertial acceleration, Extended Abstract, *32, Sitzung der Arbeitsgruppe Seismologie des FKPE,* Haidhof, Germany.

Foti, S., 2000. Multistation methods for geotechnical characterisation using surface waves, *PhD thesis,* Politecnico di Torino.

Gabriels, P., Snieder, R. & Nolet, G., 1987. *In situ* measurements of shear-wave velocity in sediments with higher-mode Rayleigh waves, *Geophys. Prospect.,* **35,** 187–196.

García-Jerez, A., Luzón, F., Sánchez-Sesma, F.J., Lunedei, E., Albarello, D., Santoyo, M.A. & Almendros, J., 2013. Diffuse elastic wavefield within a simple crustal model: some consequences for low and high frequencies, *J. geophys. Res.,* **118**(10), 5577–5595.

Gomberg, J. & Masters, T., 1988. Waveform modelling using locked-mode synthetic and differential seismograms: application to determination of the structure of Mexico, *Geophys. J. Int.,* **94,** 193–218.

Harmon, N., Forsyth, D. & Webb, S., 2007. Using ambient seismic noise to determine short-period phase velocities and shallow shear velocities in young oceanic lithosphere, *Bull. seism. Soc. Am.,* **97**(6), 2009–2023.

Havskov, J. & Singh, S.K., 1977. Shallow crustal structure below Mexico City, *Geof. Int. – Mexico,* **17,** 223–229.

Hennino, R., Tregoures, N., Shapiro, N.M., Margerin, L., Campillo, M., van Tiggelen, B. & Weaver, R., 2001. Observation of equipartition of seismic waves, *Phy. Rev. Lett.,* **86,** 3447–3450.

Hillers, G., Graham, N., Campillo, M., Kedar, S., Landes, M. & Shapiro, N.M., 2012. Global oceanic microseism sources as seen by seismic arrays and predicted by wave action models, *Geochem. Geophys. Geosyst.,* **13,** Q01021, doi:10.1029/2011GC003875.

Horike, M., 1985. Inversion of phase velocity of long-period microtremors to the *S*-wave-velocity structure down to the basement in urbanized areas, *J. Phys. Earth,* **33,** 59–96.

Iglesias, A., Clayton, R.W., Perez-Campos, X., Singh, S.K., Pacheco, J.F., Garcia, D. & Valdes-Gonzalez, C., 2010. *S* wave velocity structure below central Mexico using high-resolution surface wave tomography, *J. geophys. Res. - Solid Earth Planets,* **115,** B06307.1–B06307.10.

Koper, K., de Foy, B. & Benz, H., 2009. Composition and variation of noise recorded at the Yellowknife seismic array, 1991–2007, *J. geophys. Res.,* **114,** B10310.1–B10310.13.

Landès, M., Hubans, F., Shapiro, N.M., Paul, A. & Campillo, M., 2010. Origin of deep ocean microseisms by using teleseismic body waves, *J. geophys. Res.,* **115,** B05302, doi:10.1029/2009JB006918.

Levshin, A., Yanovskaya, T., Lander, A., Bukchin, B., Barmin, M., Ratnikova, L. & Its, E., 1989. *Seismic Surface Waves in a Laterally Inhomogeneous Earth,* Kluwer.

Lin, F.-C., Moschetti, M.P. & Ritzwoller, M.H., 2008. Surface wave tomography of the western United States from ambient seismic noise: Rayleigh and Love wave phase velocity maps, *Geophys. J. Int.,* **173,** 281–298.

Liu, X. & Fan, Y., 2012. On the characteristics of high-frequency Rayleigh waves in stratified half-space, *Geophys. J. Int.,* **190**(2), 1041–1057.

Lontsi, A.M., Sánchez-Sesma, F.J., Molina-Villegas, J.C., Ohrnberger, M. & Krüger, F., 2015. Full microtremor H/V(z, f) inversion for shallow subsurface characterization, *Geophys. J. Int.,* **202**(1), 298–312.

Malischewsky, P.G. & Scherbaum, F., 2004. Love's formula and H/V-ratio (ellipticity) of Rayleigh waves, *Wave Motion,* **40,** 57–67.

Malischewsky, P.G., Scherbaum, F. & Lomnitz, C., TranThanh, T., Wuttke, F. & Shamir, G., 2008. The domain of existence of prograde Rayleigh-wave particle motion for simple models, *Wave Motion,* **45,** 556–564.

Margerin, L., 2008. Chapter 1 Coherent Back-Scattering and Weak Localization of Seismic Waves, *Adv. Geophys.,* **50,** 1–19.

Margerin, L., Campillo, M. & Van Tiggelen, B., 2000. Multiple scattering of elastic waves, *J. geophys. Res.,* **105,** 7873–7892.

Margerin, L., Van Tiggelen, B. & Campillo, M., 2001. Effect of absorption on energy partition of elastic waves, *Bull. seism. Soc. Am.,* **91,** 624–627.

Margerin, L., Campillo, M., Van Tiggelen, B. & Hennino, R., 2009. Energy partition of seismic coda waves in layered media: theory and application to Pinyon Flats Observatory, *Geophys. J. Int.,* **177,** 571–585.

Mulargia, F., 2012. The seismic noise wavefield is not diffuse, *J. Acoust. Soc. Am.,* **131**(4), 2853–2858.

Nakamura, Y., 1989. A method for dynamic characteristics estimation of subsurface using microtremor on the ground surface, *Q. Rep. Railw. Tech. Res. Inst.,* **30,** 25–30.

Nishida, K., Kawakatsu, H. & Obara, K., 2008. Three-dimensional crustal *S* wave velocity structure in Japan using microseismic data recorded by Hi-net tiltmeters, *J. geophys. Res.,* **113,** B10302, doi:10.1029/2007JB005395.

Nolet, G. & Panza, G.F., 1976. Array analysis of seismic surface waves: limits and possibilities, *Pure appl. Geophys.,* **114,** 775–790.

O'Neill, A. & Matsuoka, T., 2005. Dominant higher surface-wave modes and possible inversion pitfalls, *J. Environ. Eng. Geophys.,* **10,** 185–201.

Pérez-Campos, X. *et al.*, 2008. Horizontal subduction and truncation of the cocos plate beneath central mexico, *Geophys. Res. Lett.,* **35,** L18303.1–L18303.6.

Perton, M., Sanchez-Sesma, F., Rodriguez-Castellanos, A., Campillo, M. & Weaver, R., 2009. Two perspectives on equipartition in diffuse elastic fields in three dimensions, *J. acoust. Soc. Am.,* **126,** 1125–1130.

Pilz, M. & Parolai, S., 2014. Statistical properties of the seismic noise field: influence of soil heterogeneities, *Geophys. J. Int.,* **199**(1), 430–440.

Poggi, V. & Fäh, D., 2010. Estimating Rayleigh wave particle motion from three-component array analysis of ambient vibrations, *Geophys. J. Int.,* **180**(1), 251–267.

Ryzhik, L., Papanicolaou, G. & Keller, J., 1996. Transport equations for elastic and other waves in random media, *Wave Motion,* **24,** 327–370.

Sánchez-Sesma, F.J. & Campillo, M., 2006. Retrieval of the Green's function from cross correlation: the canonical elastic problem, *Bull. seism. Soc. Am.,* **96**(3), 1182–1191.

Sánchez-Sesma, F.J., Pérez-Ruiz, J.A., Luzón, F., Campillo, M. & Rodriguez-Castellanos, A., 2008. Diffuse fields in dynamic elasticity, *Wave Motion,* **45,** 641–654.

Sánchez-Sesma, F.J., Rodríguez, M., Iturrarán-Viveros, U., Rodríguez-Castellanos, A., Suarez, M., Santoyo, M.A., García-Jerez, A. & Luzón, F., 2010. Site effects assessment using seismic noise, in *Proceedings of the 9th International Workshop on Seismic Microzoning and Risk Reduction*, 2010 February 21st–24th, Cuernavaca, Mexico.

Sánchez-Sesma, F.J., Weaver, R., Kawase, H., Matsushima, S., Luzón, F. & Campillo, M., 2011a. Energy partitions among elastic waves for dynamic surface loads in a semi-infinite solid, *Bull. seism. Soc. Am.,* **101,** 1704–1709.

Sánchez-Sesma, F.J. *et al.*, 2011b. A theory for microtremor H/V spectral ratio: application for a layered medium, *Geophys. J. Int.,* **186,** 221–225.

Savage, M.K., Lin, F.-C. & Townend, J., 2013. Ambient noise cross-correlation observations of fundamental and higher-mode Rayleigh wave propagation governed by basement resonance, *Geophys. Res. Lett.,* **40**(14), 3556–3561.

Shapiro, N.M. & Campillo, M., 2004. Emergence of broadband Rayleigh waves from correlations of the ambient seismic noise, *Geophys. Res. Lett.,* **31,** L07614, doi:10.1029/2004GL019491.

Shapiro, N.M., Campillo, M., Paul, A., Singh, S.K., Jongmans, D. & Sanchez-Sesma, F.J., 1997. Surface-wave propagation across the Mexican Volcanic Belt and the origin of the long-period seismic-wave amplification in the Valley of Mexico, *Geophys. J. Int.,* **128,** 151–166.

Shapiro, N.M., Campillo, M., Margerin, L., Singh, S.K., Kostoglodov, V. & Pacheco, J., 2000. The energy partitioning and the diffusive character of the seismic coda, *Bull. seism. Soc. Am.,* **90,** 655–665.

Shapiro, N.M., Singh, S.K., Almora, D. & Ayala, M., 2001. Evidence of the dominance of higher-mode surface waves in the lake-bed zone of the Valley of Mexico, *Geophys. J. Int.,* **147,** 517–527.

Shapiro, N.M., Olsen, K. & Singh, S.K., 2002. On the duration of seismic motion incident onto the Valley of Mexico for subduction zone earthquakes, *Geophys. J. Int.,* **151,** 501–510.

Shapiro, N.M., Campillo, M., Stehly, L. & Ritzwoller, M.H., 2005. High-resolution surface-wave tomography from ambient seismic noise, *Science,* **307**(5715), 1615–1618.

Singh, S.K., Quaas, R., Ordaz, M., Mooser, F., Almora, D., Torres, M. & Vasquez, R. 1995. Is there truly a hard rock site in the Valley of Mexico, *Geophys. Res. Lett.,* **22,** 481–484.

Singh, S.K., Santoyo, M., Bodin, P. & Gomberg, J., 1997. Dynamic deformation of shallow sediments in the Valley of Mexico, part II: Single-station estimates, *Bull. seism. Soc. Am.,* **87,** 540–550.

Socco, L.V. & Strobbia, C., 2004. Surface-wave method for near surface characterization: a tutorial, *Near Surf. Geophys.,* **2**(4), 165–185.

Stehly, L., Campillo, M. & Shapiro, N.M., 2006. A study of the seismic noise from its long-range correlation properties, *J. geophys. Res. - Solid Earth Planets,* **111,** B10306, doi:10.1029/2005JB004237.

Stehly, L., Fry, B., Campillo, M., Shapiro, N.M., Guilbert, J., Boschi, L. & Giardini, D., 2009. Tomography of the Alpine region from observations of seismic ambient noise, *Geophys. J. Int.,* **178**(1), 338–350.

Strollo, A., Parolai, S., Jackel, K.-H., Marzorati, S. & Bindi, D., 2008. Suitability of short-period sensors for retrieving reliable H/V peaks for frequencies less than 1 Hz, *Bull. seism. Soc. Am.,* **98**(2), 671–681.

Stutzmann, E., Schimmel, M., Patau, G. & Maggi, A., 2009. Global climate imprint on seismic noise, *Geochem. Geophys. Geosyst.,* **10,** Q11004, doi:10.1029/2009GC002619.

Suarez, M., Sánchez-Sesma, F.J., Bravo, M. & Lermo, J., 1987. *Caracteristicas de los Depositos Superficiales del Valle de México,* Instituto de Ingeneria, UNAM, Mexico.

Tanimoto, T., Ishimaru, S. & Alvizuri, C., 2006. Seasonality of particle motion of microseisms, *Geophys. J. Int.,* **166,** 253–266.

Tokimatsu, K., Tamura, S. & Kojima, H., 1992. Effects of multiple modes on Rayleigh wave dispersion, *J. Geotech. Eng.,* **118,** 1529–1543.

Tuan, T.T., Scherbaum, F. & Malischewsky, P.G., 2011. On the relationship of peaks and troughs of the ellipticity (H/V) of Rayleigh waves and the transmission response of single layer over half-space models, *Geophys. J. Int.,* **184,** 793–800.

Valdes-Gonzalez, C. & Meyer, R., 1996. Seismic structure between the Pacific coast and Mexico City from the Petatlan earthquake ($M_s = 7.6$) aftershocks, *Geof. Int. – Mexico,* **35,** 377–402.

Wathelet, M., 2005. Array recordings of ambient vibrations: surface wave inversion, *PhD thesis,* University of Liège.

Wathelet, M., 2008. An improved neighborhood algorithm: parameter conditions and dynamic scaling, *Geophys. Res. Lett.,* **35,** L09301, doi:10.1029/2008GL033256.

Weaver, R., 1982. On diffuse waves in solid media, *J. acoust. Soc. Am.,* **71,** 1608–1609.

Weaver, R., 1990. Diffusivity of ultrasound in polycrystals, *J. Mech. Phys. Solid,* **38,** 55–86.

Wielandt, E. & Forbriger, T., 1999. Near-field seismic displacement and tilt associated with the explosive activity of Stromboli, *Ann. di Geofis.,* **42**(3), 407–416.

Xia, J., Miller, R.D., Park, C.B. & Tian, G., 2003. Inversion of high frequency surface waves with fundamental and higher modes, *J. appl. Geophys.,* **52**(1), 45–57.

Yang, Y., Ritzwoller, M.H., Levshin, A.L. & Shapiro, N.M., 2007. Ambient noise Rayleigh wave tomography across Europe, *Geophys. J. Int.,* **168,** 259–274.

Yao, H., Gouédard, P., Collins, J.A., McGuire, J.J. & van der Hilst, R.D., 2011. Structure of young East Pacific Rise lithosphere from ambient noise correlation analysis of fundamental- and higher-mode Scholte-Rayleigh waves, *Comp. Rendus Geosci.,* **343**(8–9), 571–583.

Zhang, S.X. & Chan, L.S., 2003. Possible effects of misidentified mode number on Rayleigh wave inversion, *J. appl. Geophys.,* **53**(1), 17–29.